Enhanced electrochemical performances of polypyrrole/carboxyl graphene/carbon nanotubes ternary composite for supercapacitors

Haihan Zhou*, Hua-Jin Zhai**, Xiaomin Zhi

Institute of Molecular Science, Key Laboratory of Materials for Energy Conversion and Storage of Shanxi Province, Key Laboratory of Chemical Biology and Molecular Engineering of Education Ministry, Shanxi University, Taiyuan 030006, China

ARTICLE INFO

ABSTRACT

A novel strategy is proposed to obviously enhance the electrochemical capacitive properties of polypyrrole/graphene oxide/carbon nanotubes (PPy/GO/CNT) ternary composite. Here GO is treated by carboxylation reaction to obtain carboxyl graphene (CG). For comparison, PPy/GO/CNT and PPy/CG/CNT composites are synthesized with the same one-pot electro-co-deposition. Fourier transform infrared spectrometry, energy-dispersive X-ray spectroscopy, X-ray diffraction, scanning and transmission electron microscopy are carried out to characterize the composition and morphology of both composites. Unlike only utilizing the edged carboxyl groups on GO to combine with PPy coating, the current PPy/CG/CNT composite makes use of carboxyl groups distributed on basal planes and edges of CG nanosheets to combine with PPy. Accordingly, electrochemical measurements indicate that the PPy/CG/CNT electrodes markedly improve the supercapacitive properties compared to PPy/GO/CNT electrodes. The as-prepared PPy/CG/CNT composite electrodes show a high areal specific capacitance of $196.7 \, \text{mF cm}^{-2}$ at the current density of $0.5 \, \text{mA cm}^{-2}$ and superior rate capability, as well as achieve 98.1% of capacitance retention after 5000 CV cycles. The PPy/CG/CNT ternary composite we have developed holds promise for high-efficiency supercapacitor applications.

1. Introduction

Electrochemical capacitors are also known as ultracapacitors or supercapacitors, because they deliver much larger energy densities than conventional capacitors. Supercapacitors have triggered numerous studies owing to their attractive advantages of longer cycle life and higher power capability than batteries [1,2]. These characteristics enable their applications in fields such as wearable electronic devices, hybrid electric vehicles, and digital communication [3–5]. Supercapacitors can be classified into pseudocapacitors, electric double-layer capacitors (EDLCs), and hybrid capacitors. The pseudocapacitors involve Faradaic redox process during charging/discharging, usually using transition metal oxides and conducting polymers (CPs) as electrode materials. More strictly, true pseudocapacitors do not include in its constitution electrodes with a battery-type electrochemical signature. The EDLCs store energy based on electrostatic charge accumulation at the electrode-electrolyte interface, and carbon materials are often utilized as the electrode materials [6,7]. The hybrid supercapacitors are two-electrode assemblies, wherein one electrode is a battery-type faradaic electrode, and the other is a capacitive/EDLC electrode material. Generally, pseudocapacitor electrode materials show high specific energy density, but poor cycle performance; whereas EDLCs electrode materials have high specific power density and cycling stability, but relatively low energy density [8,9]. To combine the advantages of various electrode materials, considerable current research efforts are focused on the exploration of composite electrode materials, aiming for high-efficiency supercapacitor applications [10–12].

Among pseudocapacitive materials, polypyrrole (PPy), one kind of CPs, has been extensively investigated as a very promising electrode material for supercapacitors. It has a number of advantages: large theoretical specific capacitance, low cost, high electrical conductivity, and environmental friendliness [13]. However, the poor cycle life of PPy restricts its further applications, which is associated with the swelling and shrinkage during charging/discharging, due to the doping/de-doping of counter anions. Moreover, PPy shows a compact morphology owing to its dense growth, limiting the contact of electrolyte with the interior sites of polymer

---

[14,15]. Graphene oxide (GO) with large surface area, possessing abundant oxygen-containing groups (including epoxide, hydroxyl, carboxyl groups, and carbonyl), features negative charge surface and high dispersibility in water [16,17].

In recent years, PPy/GO composites have attracted great interest due to their enhanced capacitive performances relative to individual PPy [18−25], whereas the insulating GO in the composites still hinder their electrochemical capacitive performances. Chang et al. therefore electrochemically synthesized PPy/graphene composite by further reduction of GO to improve the supercapacitive performances of PPy/GO [26]. However, further reduction for GO led to relatively complicated preparation procedures, and the study suggested that the electrochemical capacitive properties of PPy/GO composite were less boosted. We thus developed a method in a recent work to prepare the PPy/GO/CNT ternary composite by one-step electrochemical co-deposition [27]. Thereinto, the GO with anionic nature and carboxyl-functionalized CNT acted as the counter ions/dopants for the charge balancing of the PPy, and meanwhile served as charge carriers in deposition bath. Note that carboxylated CNT still has a high electrical conductivity [28]. As a consequence, the introduction of CNT obviously enhanced the electrochemical capacitive properties of PPy/GO composite. Now the question is: can we push further along this line? It is known that GO shows the anionic nature due to its negative charge surface, which is primarily caused by the ionization of the carboxyl groups on it. The carboxyl groups therefore serve as the active sites on the GO nanosheets for PPy polymerization during electrodeposition. However, apart from plenty of hydroxyl (−OH) and epoxy groups (C−O−C) on the basal planes, GO sheets only have lesser carboxyl groups (−COOH) located at the edges [29]. In other words, GO as counter anions in the PPy/GO/CNT composite only utilizes the carboxyl groups located at the edges to combine with PPy, leaving quantities of oxygen-containing functional groups like −OH and C−O−C on its basal planes intact. In addition, previous studies indicated that the presence of anionic micelles improved structural properties of the resulting conducting polymer coatings [30,31]. For instance, the robust poly(3,4-ethylenedioxythiophene (PEDOT)-based films of high charge propagation dynamics were produced by introducing the carboxylate-containing 4-(pyrrole-1-yl) benzoic acid (PyBA), and the overall stability was promoted. Therefore, it is likely to enhance the electrochemical performances of PPy/GO/CNT composite by introducing more carboxyl groups-containing CG sheets.

In this study, CG acted as a new dopant to obviously enhance the supercapacitive performances of PPy based ternary composite, by making full use of carboxyl groups distributed on basal planes and edges of CG sheets to combine with more PPy with large pseudo-capacitance. Herein, CG was obtained from GO through the treatment of carboxylation, during which −OH and C−O−C located at basal planes of GO sheets were converted to −COOH. PPy/CG/CNT and PPy/GO/CNT ternary composite electrodes were fabricated using the same one-pot electro-co-deposition procedure. Electrochemical measurements indicate that PPy/CG/CNT composite has obviously improved supercapacitive performances relative to PPy/GO/CNT.

2. Experimental

2.1. Carboxylation of GO and CNTs

As schematically illustrated in Fig. 1, CG was synthesized by carboxylation of GO, and the latter was prepared by the oxidation of graphite powder according to a modified Hummers method [32,33]. For carboxylation of GO [34,35], 50 mL of aqueous suspension of GO (2 mg mL^{-1}) was adequately ultrasonicated to give a

clear suspension. After that, chloroacetic acid (5.0 g) and NaOH (6.0 g) were added to the GO aqueous suspension and reacted under ultrasonication for 2 h. The resulting CG suspension was neutralized, filtered, and washed several times with deionized water (DW) to remove the excess reactant and dried at 50 °C in vacuum oven for 24 h. For carboxylation of CNTs, pristine multi-walled CNTs were pretreated in 3 M HNO$_3$ at 140 °C under magnetic stirring by refluxing for 72 h. Subsequently, they were transferred into a mixture of concentrated H$_2$SO$_4$ and HNO$_3$ (volume ratio 3:1) and functionalized with carboxyl groups in the mixture under bath-sonication at 40 °C for 2 h. Finally, the resultant carboxylated CNTs (or CNT-COOH) were rinsed with abundant DW until the pH reached about 6.0 and dried at 60 °C for 1 day.

2.2. Electrode preparations

PPy/CG/CNT electrodes were prepared through electrochemical co-deposition in the aqueous deposition bath composed of pyrrole (0.2 M), CG (1.0 mg mL^{-1}), and carboxylated CNTs (1.0 mg mL^{-1}), which was adequately dispersed by stirring and ultrasonication prior to use. Electrodeposition was performed using a galvanostatic mode with 1 mA cm^{-2} for 1800 s in the three-electrode system. Thereinto, graphite papers, whose conductive areas are 1 cm × 1 cm, were used as the electrodeposition substrate, and saturated calomel electrode (SCE) and Pt sheet were employed as reference electrode and counter electrode, respectively. For comparison, the same electrodeposition procedure was applied to fabricate PPy/GO/CNT electrodes with the aqueous deposition bath consisting of pyrrole (0.2 M), GO (1.0 mg mL^{-1}), and carboxylated CNTs (1.0 mg mL^{-1}). Likewise, PPy/CG and PPy/CNT electrodes were obtained using aqueous deposition bath containing pyrrole (0.2 M) and CG (2.0 mg mL^{-1}) and carboxylated CNTs (2.0 mg mL^{-1}), respectively.

2.3. Physicochemical characterization

UV−Vis spectra were acquired by UV−Vis spectrophotometer (U-3900, Hitachi). Water contact angle was tested using a drop shape analyzer (DSA 100, Krüss). XPS analysis was conducted using X-ray photoelectron spectrometer (ESCALAB 250Xi, Thermo). FT-IR spectra and XRD patterns were recorded with FT-IR spectrometer (Tensor 27, Bruker) and X-ray diffractometer (Ultima IV, Rigaku), respectively. Morphologies of samples were observed through SEM (JSM-6701F, JEOL) and TEM (JEM-2100, JEOL). EDS tests were carried out through X-ray energy dispersive spectrometer (S-4800, Hitachi). Electrochemical measurements (including CV, GCD, and EIS) of the electrodes were conducted on an electrochemical workstation (CHI 660E, Chenhua) with symmetric two-electrode configuration using 1 M KCl aqueous electrolyte. EIS were recorded at the open circuit potential with a frequency range from 100 kHz to 0.01 Hz by applying an AC sinusoid signal with 5 mV amplitude.

3. Results and discussion

3.1. Material characterizations

Fig. 2a exhibits that the GO changes from brown yellow to black for CG. Both of them present Tyndall light scattering, suggesting that the GO and CG suspensions are homogeneous colloidal dispersion in DW. Fig. 2b shows UV−vis spectra of GO and CG. Both of them have the characteristic peak at 230 nm and a shoulder peak at 300 nm, which are attributed to π−π* transition of aromatic C−C bonds and n−π* transition of C=O bonds, respectively [36]. Note that the color change from brown yellow GO to black CG results in
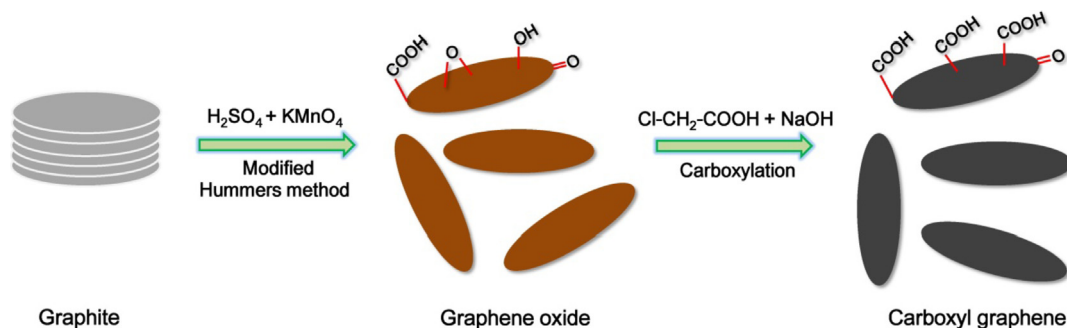
Fig. 1. Schematic representation of the preparation process for GO and CG.

an increase in UV−vis absorbance, which is caused by hydrolysis of esters and opening of epoxide rings on GO by carboxylation treatment [37]. Fig. 2c reveals that the water contact angle of CG is 40.7°, which is smaller than 56.2° of GO, indicative of better hydrophilicity for the former. This is beneficial to the access of electrolyte for CG based composites. Fig. 3 shows the C 1s XPS spectra of GO and CG. Five fitting peaks are deconvoluted for both spectra. They are C=C bond at 284.4 eV, C−C bond at 285 eV, C−O bond at 286.6 eV, C=O bond at 287.1 eV, and O−C=O bond at 288.5 eV, respectively. On the basis of the peak area, the calculated proportion of C−O bonds for GO is 43.6%, while that decreases to 29.2% for CG. Moreover, the proportion of O−C=O bonds for GO is 8.5%, while that increases to 14.0% for CG. These values suggest that carboxylation reaction led to −OH and C−O−C located at the basal plane of GO nanosheets were partially transformed into −COOH. Compared to GO, the all-round carboxyl-covered CG, including basal planes and edges, shall introduce more and relatively dispersed PPy coating into the composite during electrodeposition.

Fig. 4a presents the FT−IR spectra for GO, CG, CNT−COOH, PPy, PPy/GO/CNT, and PPy/CG/CNT. For the spectrum of GO, the characteristic peaks situated at 1729 and 1620 cm^{-1} are caused by the C=O stretching and the aromatic C=C stretching or absorbed water, respectively. Vibrations at 1227 and 1398 cm^{-1} are caused by C−OH stretching and O−H deformation, respectively. Peak at 1060 cm^{-1} is assigned to C−O stretching of alkoxy group, and the band at 852 cm^{-1} is ascribed to C−O−C [38,39]. The same characteristic peaks can be seen in the spectrum of CG, suggesting that it has the same functional groups with GO. However, the difference is that the peak at 1729 cm^{-1} ascribed to C=O stretching of carboxyl group for CG is strengthened in intensity, and meanwhile peaks at 1227 cm^{-1} attributed to hydroxy groups and 852 cm^{-1} originating from epoxy groups are weakened relative to those of GO. In accordance with XPS analysis, the FT−IR spectra of CG and GO further indicate that −OH and C−O−C on GO sheets were partially converted into −COOH by carboxylation treatment.

In the spectrum of CNT−COOH, peak at 1715 cm^{-1} is caused by C=O stretching of the carboxyl group [40], suggesting that carboxyl groups are introduced into CNTs through carboxylation treatment. The main characteristic peaks in the spectrum of PPy are assigned as follows [41,42]: 1541 cm^{-1} for C=C ring vibrations, 1457 cm^{-1} for C−C symmetric stretching, 1295 cm^{-1} for C−H in-plane stretching, 1168 cm^{-1} for C−N stretching, 1040 cm^{-1} for C−H in-plane deformation of PPy ring, and 898 and 780 cm^{-1} for N−H (wagging) and N−H (out of plane) vibrations, respectively. It can be seen from the spectra of PPy/GO/CNT and PPy/CG/CNT that both systems have the characteristic peaks of PPy, indicating that PPy exists in the composites. Nevertheless, compared to that of PPy, the absorption peak for C−H in-plane vibration at 1040 cm^{-1} has downshifted to 1031 cm^{-1} for both composites. The redshift is due to the change in chemical environment of PPy during the formation of composite, being related to electrostatic interaction between the GO or CG, CNT−COOH anions, and PPy cations [43]. In addition, the unobvious bands detected for GO, CG, and CNT−COOH in both composites could be because they are overlapped by those of PPy coating or too weak with respect to those of PPy [44].

Fig. 4b shows the XRD patterns of the PPy/CG/CNT, PPy/GO/CNT, PPy, CNT−COOH, CG, and GO samples. It can be seen that the sharp diffraction peaks for CG and GO are situated at 11.8° and 11.4°, respectively. According to the Bragg equation, their interlayer spacing were calculated to be 0.75 and 0.78 nm, respectively, which suggests that the carboxylation treatment slightly decreases the interlayer spacing of GO nanosheets. In comparison to graphite, whose interlayer distance is 0.335 nm, the increased interlayer distance of GO and CG nanosheets is related to the introduced oxygen−containing functional groups [45]. For CNT−COOH, 002 and 100 planes of graphite structure result in two diffraction peaks located at $2\theta = 26.0°$ and 42.9° [46,47], respectively. PPy reveals a broad diffraction peak, centered at $2\theta = 24.6°$, suggesting its amorphous nature [48]. PPy/GO/CNT and PPy/CG/CNT composites show the same broad diffraction peak originating from PPy. The characteristic peak associated to GO and CG disappears in the two composites, probably because the PPy coating are introduced between the layered GO and CG, increasing their interlayer spacing [19]. The disappearance of peaks of CNT−COOH in the composites is likely due to the weakening of such peaks, as well as their overlapping with PPy coating on the CNTs.

Fig. 5 (Top panels) present the SEM images of PPy/GO/CNT and PPy/CG/CNT composites. Both images show a morphology of wrinkled GO or CG nanosheets and intertwined CNTs. Meanwhile, PPy acts as coating that covers the GO or CG nanosheets, respectively, and wraps CNTs. The composites differ in that PPy/GO/CNT presents more obvious wrinkled sheet-like morphology relative to PPy/CG/CNT, which covers the wrinkled morphology of CG nanosheets. TEM images of the two composites are shown in the middle panels of Fig. 5 to reveal more morphological details. In line with SEM images, both composites show microstructure in which PPy coated GO or CG nanosheets serve as substrate to support PPy wrapped CNTs. In addition, a careful inspection and comparison for the edges of the two composites (marked with red arrows) suggests that obviously more PPy particles are present for PPy/CG/CNT composite. The bottom panels of Fig. 5 exhibit the EDS patterns of the two composites. Because of more introduced PPy, PPy/CG/CNT shows an increased atom ratio of C:O and higher atom amount of N from PPy than PPy/GO/CNT.

3.2. Electrochemical properties

A conventional two-electrode cell is used to compare the electrochemical behaviors of the as-prepared composites, allowing a
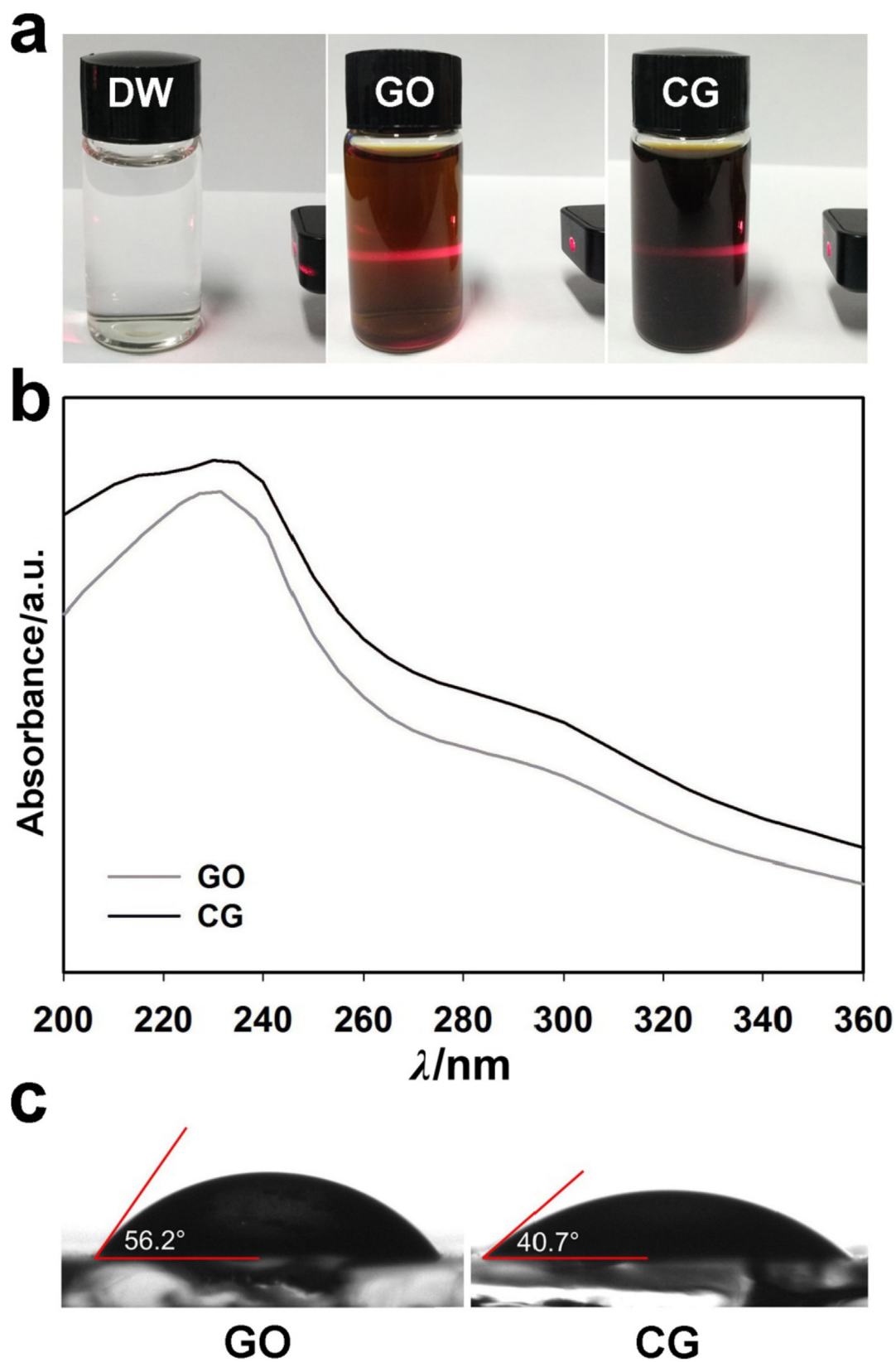
Fig. 2. (a) Tyndall scattering effect of GO and CG (1 mg mL^{-1}) dispersed in DW; (b) UV−Vis spectra for aqueous suspension of GO and CG (0.01 mg mL^{-1}); (c) Contact angle measurement for GO and CG.
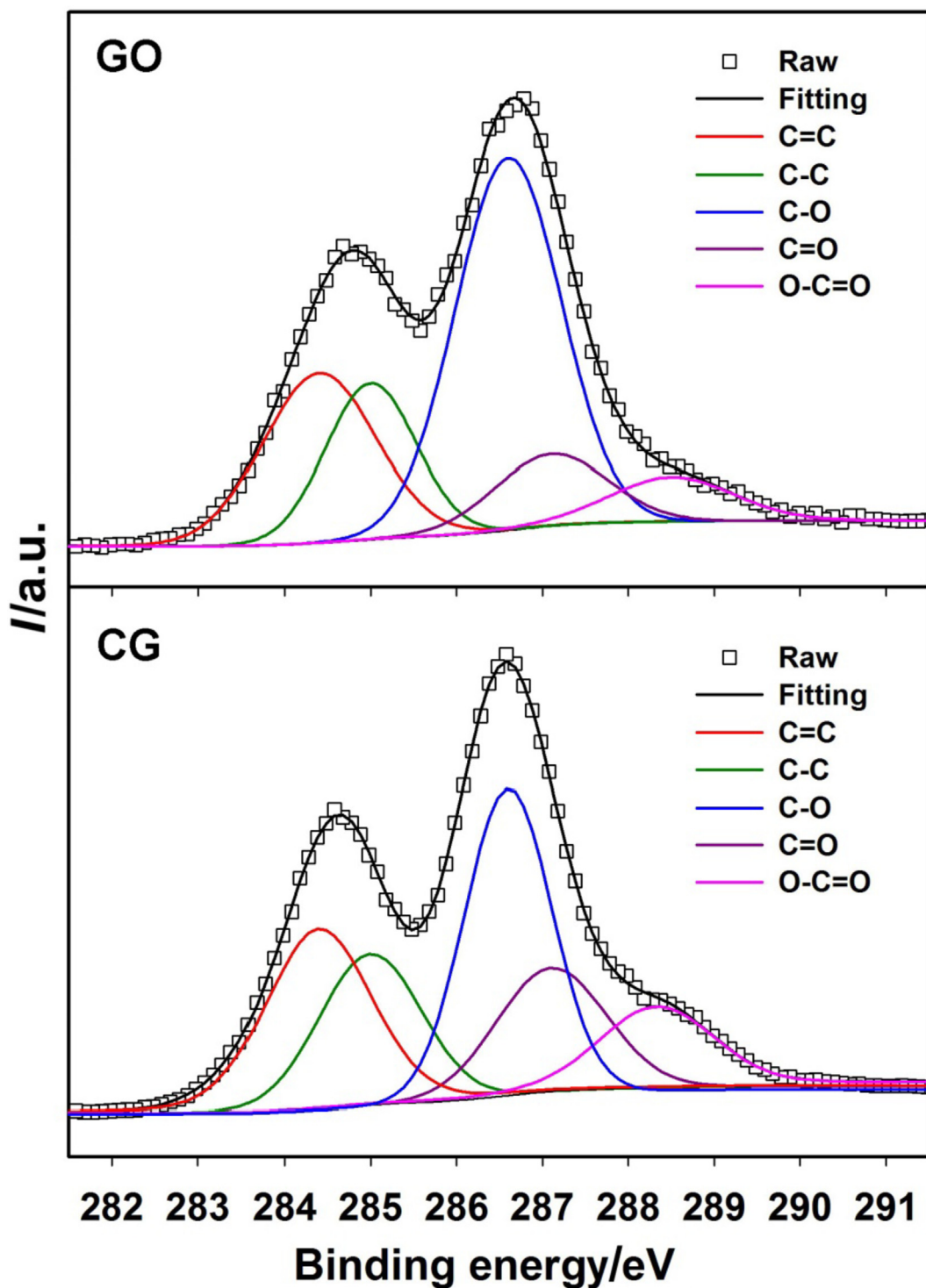
Fig. 3. C 1s XPS spectra for CG and GO.

better assessment close to practical use for supercapacitor electrodes [49]. An ideal supercapacitor electrode material should exhibit several characteristics in CV curves: high current density, rectangular shape, and good symmetry in cathodic and anodic directions [50]. Indeed, as shown in Fig. 6a, the curve of PPy/CG/CNT electrodes presents larger area and the shape closer to rectangle than those of PPy/GO/CNT, PPy/CNT, and PPy/CG electrodes at various scan rates, indicating superior capacitive behavior for PPy/

CG/CNT electrodes. Note that the CV curves of PPy/CG/CNT electrodes maintain rectangle-like shape up to $100\,\mathrm{mV\,s^{-1}}$, suggesting the good rate capability. In this study, supercapacitive performances of electrodes are assessed using areal specific capacitance (C_S), which is usually adopted as supercapacitors are applied in small scale or stationary electronic devices [51,52]. The C_S (in F $\mathrm{cm^{-2}}$) can be obtained on the basis of the CV curves through the following equation: $C_S = \int I\,dV/(v \times \Delta V \times S)$, herein $\int I\,dV$ is the
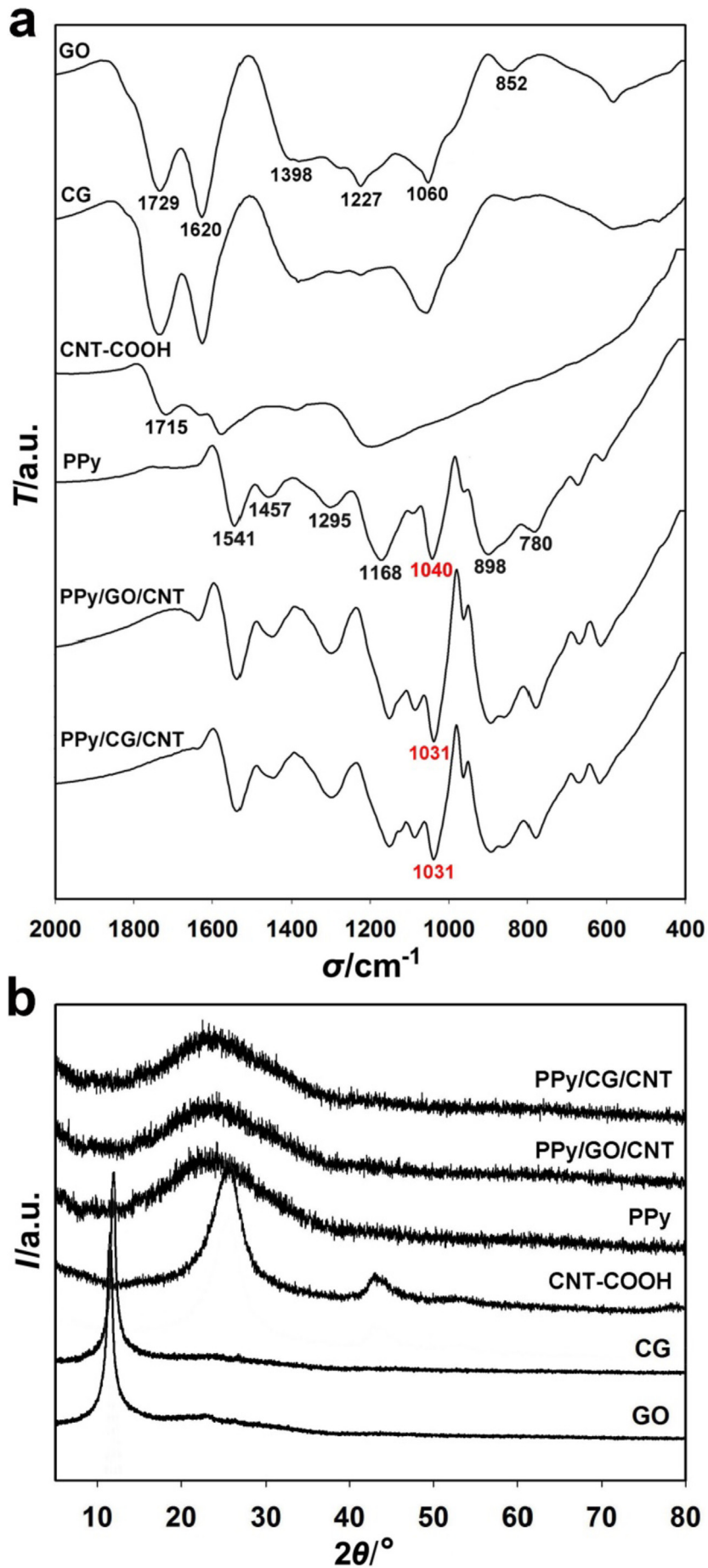
Fig. 4. (a) FT-IR spectra for GO, CG, carboxylated CNT, PPy, PPy/GO/CNT, and PPy/CG/CNT; (b) XRD patterns for PPy/CG/CNT, PPy/GO/CNT, PPy, CNT-COOH, CG, and GO.
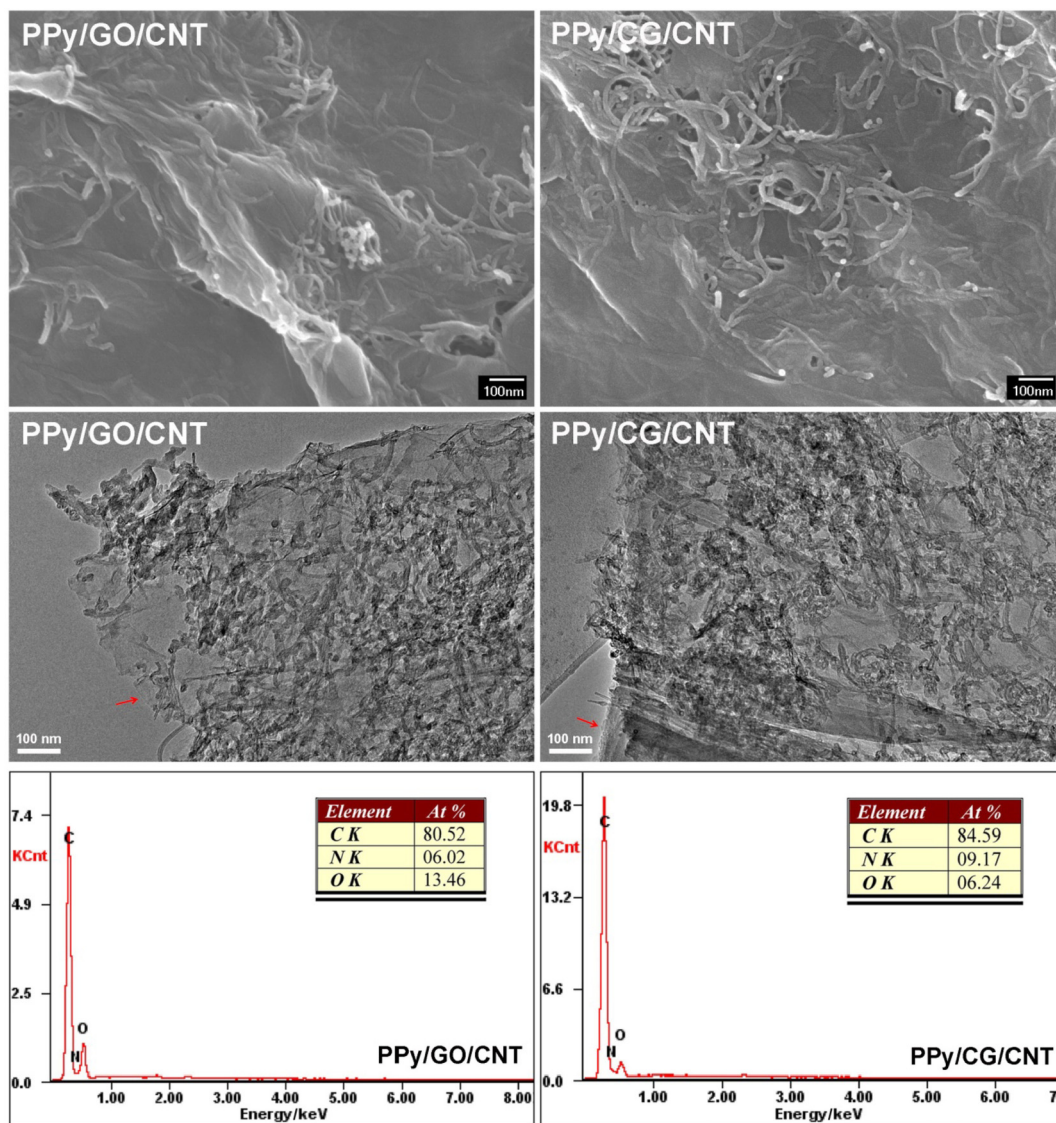
Fig. 5. SEM images (top panels), TEM images (middle panels), and EDS patterns (bottom panels) of PPy/GO/CNT and PPy/CG/CNT composites.

integrated area for the CV curve; ν the scan rate in V s^{-1}; ΔV the potential window tested in V, and S the surface area of active material (i.e. the geometric surface area of the collector electrode, which is fixed at 1 cm^2 in this study). Fig. 6b reveals that PPy/CG/CNT has the highest C_S at various scan rates, indicating the obviously enhanced capacitive performances for the ternary composite by introducing CG. In addition, compared with binary PPy/CNT and PPy/CG composites, the promoted properties for PPy/CG/CNT composite can be attributed to the factors that the introduced CG and CNT increase the specific surface area and electrical conductivity for the binary composites, respectively.

The electrochemical capacitive properties of PPy/CG, PPy/CNT, PPy/GO/CNT and PPy/CG/CNT composite electrodes are further compared via GCD measurements. As shown in Fig. 6c, the 0.5 and 1.0 mA cm^{-2} plots for all electrodes present triangle shape, and yet the PPy/CG/CNT electrodes exhibit longer discharging time. The columbic efficiency (η) of electrodes is defined as the ratio of discharge time to charge time [53]. The η value at 0.5 mA cm^{-2} for PPy/CG/CNT is calculated to be 97.2%, which is larger than 94.9% for PPy/GO/CNT, 93.8% for PPy/CNT, and 93.1% for PPy/CG. Low IR drop is crucial for supercapacitors, because it will decrease the

production of unwanted heat during the charge-discharge process [54]. The plots at 1.0 mA cm^{-2} reveal that PPy/CG/CNT electrodes have the lowest IR drop, suggesting that supercapacitor cell composed of PPy/CG/CNT electrodes have the smallest internal resistance.

The C_S of single electrodes is obtained based on GCD curves using the following equation: $C_S = (2 \times I \times t)/(\Delta V \times S)$, where I is the discharge current in A, t the discharge time in s, ΔV the potential window tested in V, and S the surface area of active material (i.e. the geometric surface area of the collector electrode) in cm^2. Fig. 6d shows that PPy/CG/CNT electrodes have obviously higher C_S than PPy/GO/CNT, PPy/CNT, and PPy/CG electrodes at different current densities. Herein, at 0.5 mA cm^{-2}, PPy/GO/CNT electrodes achieve a C_S of 170.4 mF cm^{-2}, whereas the C_S of PPy/CG/CNT electrodes rises to as high as 196.7 mF cm^{-2}. The latter value is also larger than those of other electrode materials reported recently based on CPs like PEDOT/Prussian blue/H−TiO$_2$ (40.0 mF cm^{-2}) [55], PPy/polyoxometalate (77.0 mF cm^{-2}) [56], graphene/PANI-graphene hybrid (190.6 mF cm^{-2}) [57], three-dimensional porous PANI/graphene (67.2 mF cm^{-2}) [58], PEDOT/rGO (43.75 mF cm^{-2}) [59], and PANI/graphite oxide hybrid

$(6.3 \, \text{mF} \, \text{cm}^{-2})$ [51]. Further observation in Fig. 6d indicates that the C_S of PPy/CG/CNT electrodes shows a trend of relatively smooth decline as compared to that of PPy/GO/CNT electrodes as the current density increases. Here PPy/CG/CNT composite maintains 71.3% of initial capacitance as the GCD current density increases from 0.5 to $10 \, \text{mA} \, \text{cm}^{-2}$, whereas PPy/GO/CNT composite only retains 58.2%. These numbers indicate that PPy/CG/CNT composite has distinctly boosted rate capability.

Electrochemical properties of the electrodes are compared by EIS characterizations to further confirm the superiority of PPy/CG/CNT relative to PPy/GO/CNT as supercapacitor electrode material. The obtained Nyquist plots of the electrodes are illustrated in Fig. 7. Both impedance plots display the vertical trend at low frequencies, demonstrating their capacitive behavior. However, PPy/CG/CNT electrodes show better capacitive character, because the more vertical the plot, the more like an ideal capacitor the supercapacitor [60]. The intercept at x-axis in Nyquist plots represents the equivalent series resistance (ESR) [61]. Fig. 7 (inset) exhibits that PPy/CG/CNT electrodes $(4.0 \, \Omega)$ have lower ESR than PPy/GO/CNT electrodes $(6.6 \, \Omega)$. This is a key specification to electrochemical energy-storing devices because ESR is an important factor that affects the power density [60]. Thus, EIS measurements further confirm the superior supercapacitive performances for PPy/CG/CNT electrodes with respect to PPy/GO/CNT electrodes. This can be ascribed to the introduction of more polymerized PPy coating with high pseudocapacitance and their more dispersed distribution in PPy/CG/CNT composite. Herein CG takes full advantage of carboxyl groups distributed on basal and edged planes of nanosheets to combine with more PPy coating, in contrast to only carboxyl groups restricted on the edges for GO. Moreover, more hydrophilic CG nanosheets promote the wettability of the composite, enabling

aqueous electrolyte to access more easily.

3.3. Cycling stability and Ragone plot

The cycling stability of electrode materials is an imperative performance to evaluate their potential for practical uses. Fig. 8a shows the cycling stability of PPy/GO/CNT and PPy/CG/CNT electrodes using CV tests at $80 \, \text{mV} \, \text{s}^{-1}$ for 5000 cycles. During initial cycles, the stability tests result in an increase of specific capacitance for both composite electrodes. This is because hydrophilic GO or CG within both composites induce the surface gradual wetting during cycling, thereby resulting in more electroactive surface area [62]. PPy/CG/CNT and PPy/GO/CNT electrodes maintain 98.1% and 96.5% of initial capacitance after 5000 cycles, respectively, indicative of excellent cycling stability for both composites. It is well known that PPy commonly exhibits a poor cycle life, because the doping/dedoping of counter anions leads to swelling/shrinkage of PPy [15]. Thus the excellent cycling stability for both PPy/CG/CNT and PPy/GO/CNT composites is impressive. It can be attributed to the fact that the introduced GO or CG nanosheets and CNTs provide mechanical support, simultaneously allowing space for swelling and shrinkage of PPy. The higher stability for PPy/CG/CNT electrodes is likely related to the relatively dispersed PPy coating introduced and better hydrophilicity for CG as well, which is favourable for improving the wettability of composite to electrolyte during cycling.

Areal energy density (E) and power density (P) for the tested symmetric supercapacitor consisting of PPy/CG/CNT electrodes are calculated based on the GCD curves through the following equations [51], respectively: $E = (1/2 \times C_{S,cell} \Delta V^2)/3600$ and $P = 3600 \times E/t$, where ΔV is the tested potential window (V), $C_{S,cell}$
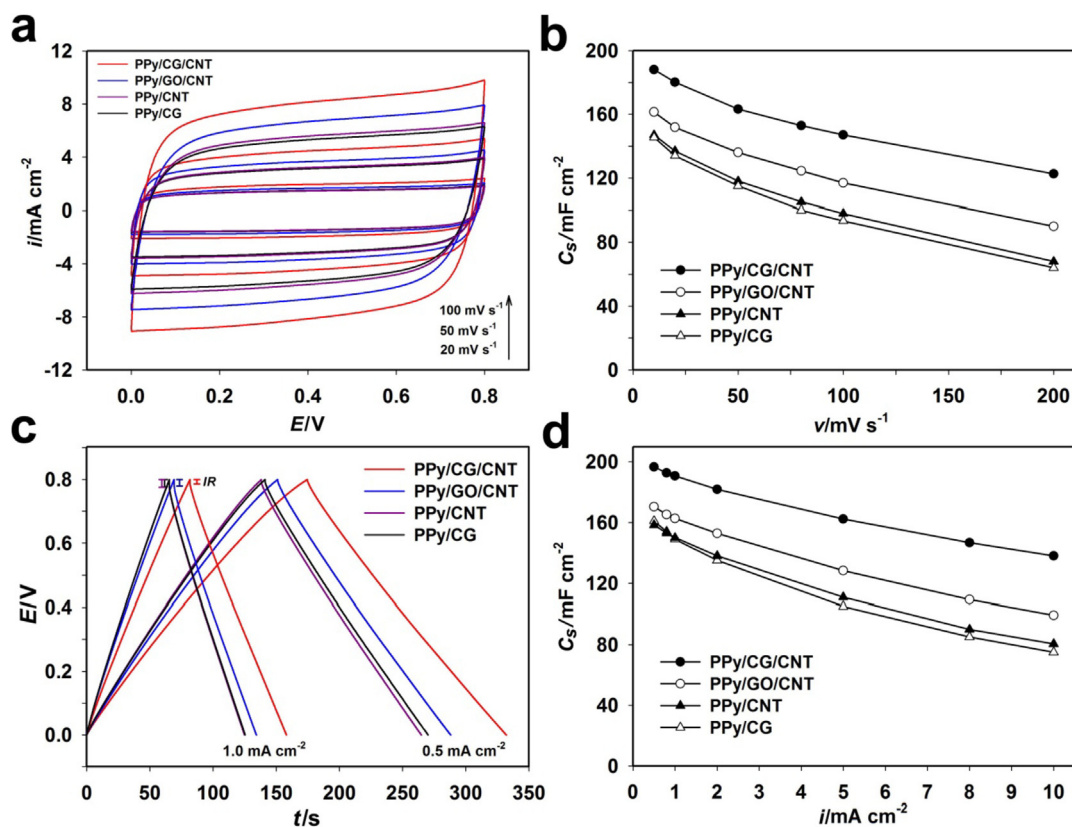

Fig. 6. (a) CV curves at 20, 50, and $100 \, \text{mV} \, \text{s}^{-1}$, (b) areal specific capacitance as a function of CV scan rate, (c) GCD curves at 0.5 and $1.0 \, \text{mA} \, \text{cm}^{-2}$, and (d) plots of areal specific capacitance *vs.* GCD current densities for PPy/CG, PPy/CNT, PPy/GO/CNT, PPy/CG/CNT composite electrodes.

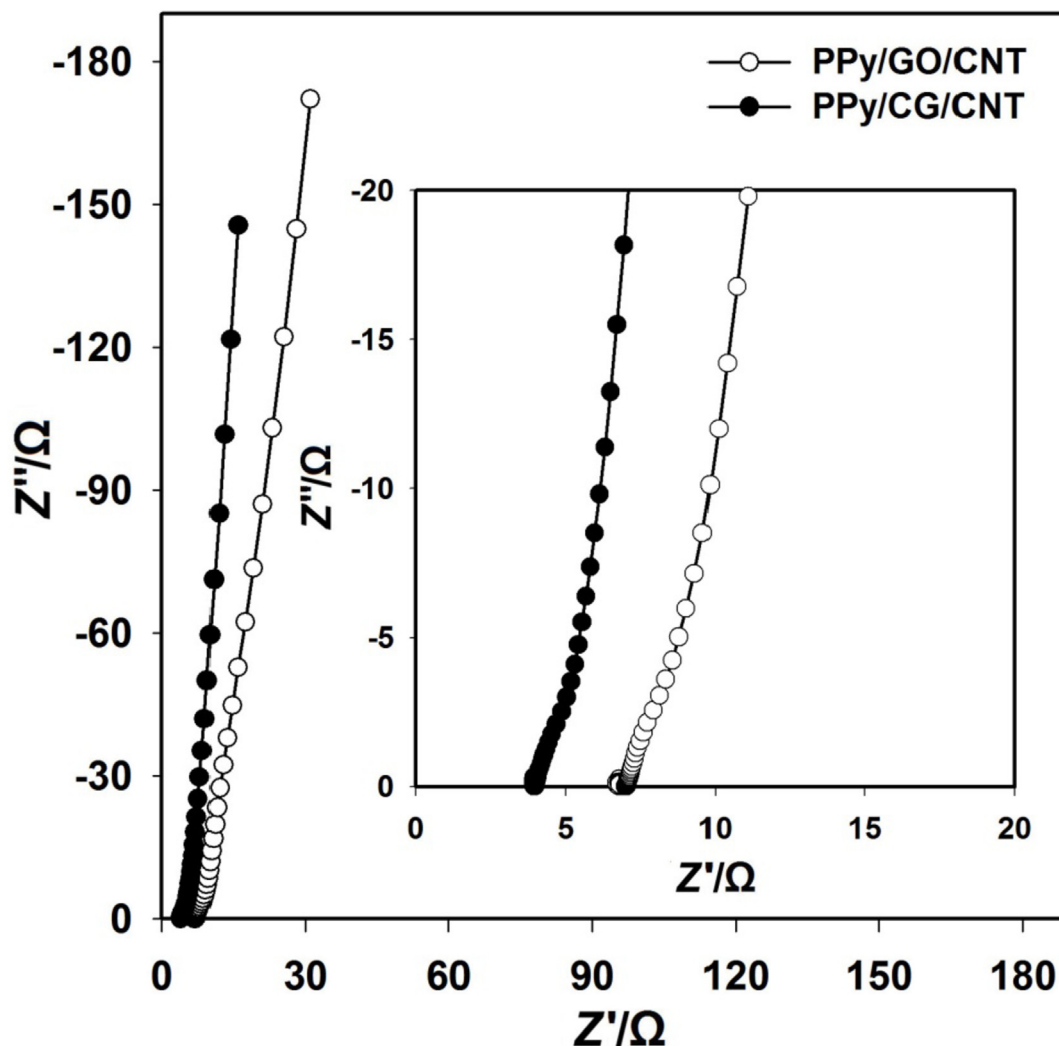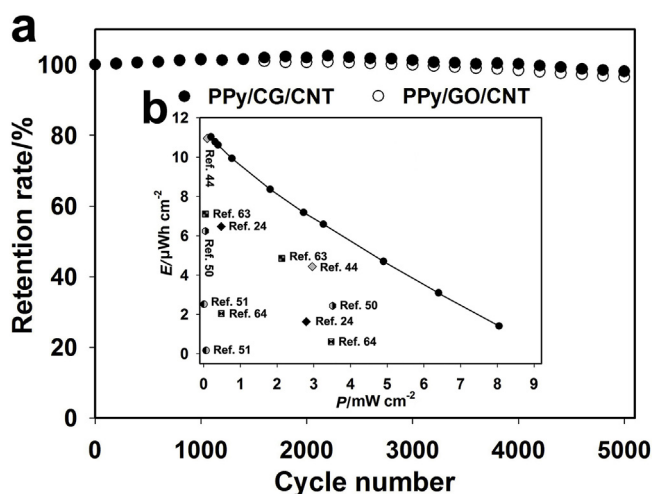**Fig. 7.** EIS Nyquist plots for the PPy/GO/CNT and PPy/CG/CNT electrodes.

Fig. 8. (a) Cycle performance tested by CV at $80\,mV\,s^{-1}$ for PPy/GO/CNT and PPy/CG/CNT electrodes; (b) Ragone plot of supercapacitor consisting of symmetric PPy/CG/CNT electrodes, including the values for other CPs based supercapacitors reported.

the areal capacitance of supercapacitor (F cm^{-2}), and t the discharge time (s). Fig. 8b exhibits the obtained Ragone plot, in which the supercapacitor cell consisting of PPy/CG/CNT electrodes delivers the maximum E ($10.9\,\mu Wh\,cm^{-2}$) and the largest P ($8.1\,mW\,cm^{-2}$) at 0.5 and $30\,mA\,cm^{-2}$, respectively. These values are higher than other CPs based supercapacitors reported recently including PPy/GO [24], PPy/CNTs [44], GO/PEDOT [50], PANI/graphite oxide [51], CNTs/PEDOT [63], and carbon paper/PPy [64], which enable the PPy/CG/CNT composite to be used as an electrode material for high-efficiency supercapacitors.

4. Conclusions

PPy/CG/CNT ternary composite has been fabricated as a supercapacitor electrode material via one-pot co-electrodeposition. In contrast to PPy/GO/CNT ternary composite, PPy/CG/CNT takes full advantage of carboxyl groups distributed on basal planes and edges of CG nanosheets to combine with PPy coating, resulting in obviously improved supercapacitive performances. The improvement is associated to the introduction of more PPy coating with large pseudo-capacitance and more hydrophilic CG nanosheets. The PPy/

CG/CNT composite electrodes deliver high specific capacitance ($196.7 \, \text{mF cm}^{-2}$ at $0.5 \, \text{mA cm}^{-2}$) and superior rate capability. Furthermore, after 5000 CV cycles, the PPy/CG/CNT electrodes retain 98.1% of the initial capacitance. The present results make PPy/CG/CNT ternary composite very promising for high-efficiency supercapacitor applications.

Acknowledgments

References

[1] D. Sheberla, J.C. Bachman, J.S. Elias, C.J. Sun, Y. Shao-Horn, M. Dincă, Conductive MOF electrodes for stable supercapacitors with high areal capacitance, Nat. Mater. 16 (2017) 220–224.

[2] M.S. Zhu, Y. Huang, Y. Huang, H.F. Li, Z.F. Wang, Z.X. Pei, Q. Xue, H.Y. Geng, C.Y. Zhi, A highly durable, transferable, and substrate-versatile high-performance all-polymer micro-supercapacitor with plug-and-play function, Adv. Mater. 29 (2017), 1605137.

[3] Y. Zhao, L.F. Hu, S.Y. Zhao, L.M. Wu, Preparation of $MnCo_2O_4@Ni(OH)_2$ core-shell flowers for asymmetric supercapacitor materials with ultrahigh specific capacitance, Adv. Funct. Mater. 26 (2016) 4085–4093.

[4] T.Y. Choi, B.U. Hwang, B.Y. Kim, T.Q. Trung, Y.H. Nam, D.N. Kim, K. Eom, N.E. Lee, Stretchable, transparent, and stretch-unresponsive capacitive touch sensor array with selectively patterned silver nanowires/reduced graphene oxide electrodes, ACS Appl. Mater. Interfaces 9 (2017) 18022–18030.

[5] T. Zhai, X.H. Lu, F.X. Wang, H. Xia, Y.X. Tong, MnO_2 nanomaterials for flexible supercapacitors: performance enhancement via intrinsic and extrinsic modification, Nanoscale Horiz. 1 (2016) 109–124.

[6] J. Chao, J.W. Deng, W.J. Zhou, J.W. Liu, R.Z. Hu, L.C. Yang, M. Zhu, O.G. Schmidt, Hierarchical nanoflowers assembled from MoS_2/polyaniline sandwiched nanosheets for high-performance supercapacitors, Electrochim. Acta 243 (2017) 98–104.

[7] S.H. Yue, H. Tong, L. Lu, W.W. Tang, W.L. Bai, F.Q. Jin, Q.W. Han, J.P. He, J. Liu, X.G. Zhang, Hierarchical $NiCo_2O_4$ nanosheets/nitrogen doped graphene/carbon nanotube film with ultrahigh capacitance and long cycle stability as a flexible binder-free electrode for supercapacitors, J. Mater. Chem. A 5 (2017) 689–698.

[8] Y.Z. Chen, W.K. Pang, H.H. Bai, T.F. Zhou, Y.N. Liu, S. Li, Z.P. Guo, Enhanced structural stability of nickel-cobalt hydroxide via intrinsic pillar effect of metaborate for high-power and long-life supercapacitor electrodes, Nano Lett. 17 (2017) 429–436.

[9] D.Z. Zheng, H.B. Feng, X.Y. Zhang, X.J. He, M.H. Yu, X.H. Lu, Y.X. Tong, Porous MoO_2 nanowires as stable and high-rate negative electrodes for electrochemical capacitors, Chem. Commun. 53 (2017) 3929–3932.

[10] C. Zhao, X. Shao, Z. Zhu, C. Zhao, X. Qian, One-pot hydrothermal synthesis of RGO/FeS composite on Fe foil for high performance supercapacitors, Electrochim. Acta 246 (2017) 497–506.

[11] P.P. Shi, L. Li, L. Hua, Q.Q. Qian, P.F. Wang, J.Y. Zhou, G.Z. Sun, W. Huang, Design of amorphous manganese oxide@multiwalled carbon nanotube fiber for robust solid-state supercapacitor, ACS Nano 11 (2017) 444–452.

[12] S. Kong, K. Cheng, T. Ouyang, Y. Gao, K. Ye, G. Wang, D. Cao, Facile electrodepositing processed of RuO_2-graphene nanosheets-CNT composites as a binder-free electrode for electrochemical supercapacitors, Electrochim. Acta 246 (2017) 433–442.

[13] X.W. Yang, Z.X. Lin, J.X. Zheng, Y.J. Huang, B. Chen, Y.Y. Mai, X.L. Feng, Facile template-free synthesis of vertically aligned polypyrrole nanosheets on nickel foams for flexible all-solid-state asymmetric supercapacitors, Nanoscale 8 (2016) 8650–8657.

[14] M.S. Zhu, Y. Huang, Q.H. Deng, J. Zhou, Z.X. Pei, Q. Xue, Y. Huang, Z.F. Wang, H.F. Li, Q. Huang, C.Y. Zhi, Highly flexible, freestanding supercapacitor electrode with enhanced performance obtained by hybridizing polypyrrole chains with MXene, Adv. Energy Mater. 6 (2016), 1600969.

[15] G.A. Snook, P. Kao, A.S. Best, Conducting-polymer-based supercapacitor devices and electrodes, J. Power Sources 196 (2011) 1–12.

[16] S. Lehtimäki, M. Suominen, P. Damlin, S. Tuukkanen, C. Kvarnström, D. Lupo, Preparation of supercapacitors on flexible substrates with electrodeposited PEDOT/Graphene composites, ACS Appl. Mater. Interfaces 7 (2015) 22137–22147.

[17] H.L. Wang, Q.L. Hao, X.J. Yang, L.D. Lu, X. Wang, Effect of graphene oxide on the properties of its composite with polyaniline, ACS Appl. Mater. Interfaces 2

[18] W.L. Wu, L.Q. Yang, S.L. Chen, Y.M. Shao, L.Y. Jing, G.H. Zhao, H. Wei, Core-shell nanospherical polypyrrole/graphene oxide composites for high performance supercapacitors, RSC Adv. 5 (2015) 91645–91653.

[19] C.Z. Zhu, J.F. Zhai, D. Wen, S.J. Dong, Graphene oxide/polypyrrole nanocomposites: one-step electrochemical doping, coating and synergistic effect for energy storage, J. Mater. Chem. 22 (2012) 6300–6306.

[20] L.Q. Fan, G.J. Liu, J.H. Wu, L. Liu, J.M. Lin, Y.L. Wei, Asymmetric supercapacitor based on graphene oxide/polypyrrole composite and activated carbon electrodes, Electrochim. Acta 137 (2014) 26–33.

[21] J.Y. Cao, Y.M. Wang, J.C. Chen, X.H. Li, F.C. Walsh, J.H. Ouyang, D.C. Jia, Y. Zhou, Three-dimensional graphene oxide/polypyrrole composite electrodes fabricated by one-step electrodeposition for high performance supercapacitors, J. Mater. Chem. A 3 (2015) 14445–14457.

[22] I.M.D. Salas, Y.N. Sudhakar, M. Selvakumar, High performance of symmetrical supercapacitor based on multilayer films of graphene oxide/polypyrrole electrodes, Appl. Surf. Sci. 296 (2014) 195–203.

[23] J. Li, H.Q. Xie, Y. Li, Fabrication of graphene oxide/polypyrrole nanowire composite for high performance supercapacitor electrodes, J. Power Sources 241 (2013) 388–395.

[24] H.H. Zhou, G.Y. Han, Y.M. Xiao, Y.Z. Chang, H.J. Zhai, Facile preparation of polypyrrole/graphene oxide nanocomposites with large areal capacitance using electrochemical codeposition for supercapacitors, J. Power Sources 263 (2014) 259–267.

[25] K. Qi, Y.B. Qiu, X.P. Guo, Pulse electrochemical incorporation of graphene oxide into polypyrrole films for supercapacitor electrode materials, Electrochim. Acta 137 (2014) 685–692.

[26] H.H. Chang, C.K. Chang, Y.C. Tsai, C.S. Liao, Electrochemically synthesized graphene/polypyrrole composites and their use in supercapacitor, Carbon 50 (2012) 2331–2336.

[27] H.H. Zhou, G.Y. Han, One-step fabrication of heterogeneous conducting polymers-coated graphene oxide/carbon nanotubes composite films for high-performance supercapacitors, Electrochim. Acta 192 (2016) 448–455.

[28] P. Liu, X. Wang, H.D. Li, Preparation of carboxylated carbon nanotubes/polypyrrole composite hollow microspheres via chemical oxidative interfacial polymerization and their electrochemical performance, Synth. Met. 181 (2013) 72–78.

[29] S. Park, R.S. Ruoff, Chemical methods for the production of graphenes, Nat. Nanotechnol. 4 (2009) 217–224.

[30] L. Adamczyk, P.J. Kulesza, Fabrication of composite coatings of 4-(pyrrole-1-yl) benzoate-modified poly-3,4-ethylenedioxythiophene with phosphomolybdate and their application in corrosion protection, Electrochim. Acta 56 (2011) 3649–3655.

[31] M. Gierwatowska, B. Kowalewska, J.A. Cox, P.J. Kulesza, Multifunctional mediating system composed of a conducting polymer matrix, redox mediator and functionalized carbon nanotubes: integration with an enzyme for effective bioelectrocatalytic oxidation of glucose, Electroanalysis 25 (2013) 2651–2658.

[32] W.S. Hummers, R.E. Offeman, Preparation of graphitic oxide, J. Am. Chem. Soc. 80 (1958), 1339–1339.

[33] Y.X. Xu, H. Bai, G.W. Lu, C. Li, G.Q. Shi, Flexible graphene films via the filtration of water-soluble noncovalent functionalized graphene sheets, J. Am. Chem. Soc. 130 (2008) 5856–5857.

[34] X.M. Sun, Z. Liu, K. Welsher, J.T. Robinson, A. Goodwin, S. Zaric, H.J. Dai, Nano-graphene oxide for cellular imaging and drug delivery, Nano Res. 1 (2008) 203–212.

[35] Z. Hu, J. Li, C.Y. Li, S.J. Zhao, N. Li, Y.F. Wang, F. Wei, L. Chen, Y.D. Huang, Folic acid-conjugated graphene-ZnO nanohybrid for targeting photodynamic therapy under visible light irradiation, J. Mater. Chem. B 1 (2013) 5003–5013.

[36] K. Zhang, N. Heo, X. Shi, J.H. Park, Chemically modified graphene oxide-wrapped quasi-micro Ag decorated silver trimolybdate nanowires for photocatalytic applications, J. Phys. Chem. C 117 (2013) 24023–24032.

[37] R. Imani, S.H. Emami, S. Faghihi, Nano-graphene oxide carboxylation for efficient bioconjugation applications: a quantitative optimization approach, J. Nanoparticle Res. 17 (2015) 88.

[38] M. Bagherzadeh, Z.S. Ghahfarokhi, E.G. Yazdi, Electrochemical and surface evaluation of the anti-corrosion properties of reduced graphene oxide, RSC Adv. 6 (2016) 22007–22015.

[39] C. Bora, S.K. Dolui, Fabrication of polypyrrole/graphene oxide nanocomposites by liquid/liquid interfacial polymerization and evaluation of their optical, electrical and electrochemical properties, Polymer 53 (2012) 923–932.

[40] S. Bhandari, M. Deepa, A.K. Srivastava, A.G. Joshi, R. Kant, Poly(3,4-ethylenedioxythiophene)-multiwalled carbon nanotube composite films: structure-directed amplified electrochromic response and improved redox activity, J. Phys. Chem. B 113 (2009) 9416–9428.

[41] C.X. Wang, G.J. Shao, Z.P. Ma, S. Liu, W. Song, J.J. Song, Constructing $Fe_3O_4@N$-rich carbon core-shell microspheres as anode for lithium ion batteries with enhanced electrochemical performance, Electrochim. Acta 130 (2014) 679–688.

[42] A. Kumar, R.K. Singh, H.K. Singh, P. Srivastava, R. Singh, Enhanced capacitance and stability of p-toluenesulfonate doped polypyrrole/carbon composite for electrode application in electrochemical capacitors, J. Power Sources 246 (2014) 800–807.

[43] A. Singh, A. Chandra, Graphite oxide/polypyrrole composite electrodes for achieving high energy density supercapacitors, J. Appl. Electrochem. 43 (2013)

773—782.

[44] H.H. Zhou, G.Y. Han, Y.M. Xiao, Y.Z. Chang, H.J. Zhai, A comparative study on long and short carbon nanotubes-incorporated polypyrrole/poly(sodium 4-styrenesulfonate) nanocomposites as high-performance supercapacitor electrodes, Synth. Met. 209 (2015) 405—411.

[45] H.L. Guo, X.F. Wang, Q.Y. Qian, F.B. Wang, X.H. Xia, A green approach to the synthesis of graphene nanosheets, ACS Nano 3 (2009) 2653—2659.

[46] S.Z. Li, Y.B. Gong, Y.C. Yang, C. He, L.L. Hu, L.F. Zhu, L.P. Sun, D. Shu, Recyclable CNTs/Fe$_3$O$_4$ magnetic nanocomposites as adsorbents to remove bisphenol A from water and their regeneration, Chem. Eng. J. 260 (2015) 231—239.

[47] Y.K. Lee, K.J. Lee, D.S. Kim, D.J. Lee, J.Y. Kim, Polypyrrole-carbon nanotube composite films synthesized through gas-phase polymerization, Synth. Met. 160 (2010) 814—818.

[48] H. Zhou, T. Ni, X.T. Qing, X.X. Yue, G. Li, Y. Lu, One-step construction of graphene-polypyrrole hydrogels and their superior electrochemical performance, RSC Adv. 4 (2014) 4134—4139.

[49] V. Khomenko, E. Frackowiak, F. Béguin, Determination of the specific capacitance of conducting polymer/nanotubes composite electrodes using different cell configurations, Electrochim. Acta 50 (2005) 2499—2506.

[50] H.H. Zhou, G.Y. Han, D.Y. Fu, Y.Z. Chang, Y.M. Xiao, H.J. Zhai, Petal-shaped poly(3,4-ethylenedioxythiophene)/sodium dodecyl sulfate-graphene oxide intercalation composites for high-performance electrochemical energy storage, J. Power Sources 272 (2014) 203—210.

[51] H.G. Wei, J.H. Zhu, S.J. Wu, S.Y. Wei, Z.H. Guo, Electrochromic polyaniline/graphite oxide nanocomposites with endured electrochemical energy storage, Polymer 54 (2013) 1820—1831.

[52] J. Li, S.S. Delekta, P. Zhang, S. Yang, M.R. Lohe, X. Zhuang, X. Feng, M. Östling, Scalable fabrication and integration of graphene microsupercapacitors through full inkjet printing, ACS Nano 11 (2017) 8249—8256.

[53] R. Bendi, V. Kumar, V. Bhavanasi, K. Parida, P.S. Lee, Metal organic framework-derived metal phosphates as electrode materials for supercapacitors, Adv. Energy Mater. 6 (2016), 1501833.

[54] S. Lalwani, V. Sahu, R.B. Marichi, G. Singh, R.K. Sharma, In situ immobilized, magnetite nanoplatelets over holey graphene nanoribbons for high performance solid state supercapacitor, Electrochim. Acta 224 (2017) 517—526.

[55] M. Szkoda, K. Trzciński, J. Rysz, M. Gazda, K. Siuzdak, A. Lisowska-Oleksiak, Electrodes consisting of PEDOT modified by Prussian Blue analogues deposited onto titania nanotubes - their highly improved capacitance, Solid State Ionics 302 (2017) 197—201.

[56] M. Yang, S.B. Hong, J.H. Yoon, D.S. Kim, S.W. Jeong, D.E. Yoo, T.J. Lee, K.G. Lee, S.J. Lee, B.G. Choi, Fabrication of flexible, redoxable, and conductive nanopillar arrays with enhanced electrochemical performance, ACS Appl. Mater. Interfaces 8 (2016) 22220—22226.

[57] K. Chi, Z.Y. Zhang, J.B. Xi, Y.A. Huang, F. Xiao, S. Wang, Y.Q. Liu, Freestanding graphene paper supported three-dimensional porous graphene-polyaniline nanocomposite synthesized by inkjet printing and in flexible all-solid-state supercapacitor, ACS Appl. Mater. Interfaces 6 (2014) 16312—16319.

[58] Q.Q. Zhou, Y.R. Li, L. Huang, C. Li, G.Q. Shi, Three-dimensional porous graphene/polyaniline composites for high-rate electrochemical capacitors, J. Mater. Chem. A 2 (2014) 17489—17494.

[59] X.L. Mao, W.Y. Yang, X. He, Y. Chen, Y.T. Zhao, Y.J. Zhou, Y.J. Yang, J.H. Xu, The preparation and characteristic of poly (3,4-ethylenedioxythiophene)/reduced graphene oxide nanocomposite and its application for supercapacitor electrode, Mater. Sci. Eng. B 216 (2017) 16—22.

[60] Y.F. Xu, I. Hennig, D. Freyberg, A.J. Strudwick, M.G. Schwab, T. Weitz, K.C.P. Cha, Inkjet-printed energy storage device using graphene/polyaniline inks, J. Power Sources 248 (2014) 483—488.

[61] P.T. Yan, J. Xu, C. Wu, Y. Gu, X.S. Zhang, R.J. Zhang, Y.B. Song, High-power supercapacitors based on hierarchical porous nanometer-sized silicon carbide-derived carbon, Electrochim. Acta 189 (2016) 16—21.

[62] H.L. Wang, C.M.B. Holt, Z. Li, X.H. Tan, B.S. Amirkhiz, Z.W. Xu, B.C. Olsen, T. Stephenson, D. Mitlin, Graphene-nickel cobaltite nanocomposite asymmetrical supercapacitor with commercial level mass loading, Nano Res. 5 (2012) 605—617.

[63] H.H. Zhou, G.Y. Han, Y.Z. Chang, D.Y. Fu, Y.M. Xiao, Highly stable multi-wall carbon nanotubes@poly(3,4-ethylenedioxythiophene)/poly(styrene sulfonate) core-shell composites with three-dimensional porous nano-network for electrochemical capacitors, J. Power Sources 274 (2015) 229—236.

[64] H.G. Wei, Y.R. Wang, J. Guo, X.R. Yan, R. O'Connor, X. Zhang, N.Z. Shen, B.L. Weeks, X.H. Huang, S.Y. Wei, Z.H. Guo, Electropolymerized polypyrrole nanocoatings on carbon paper for electrochemical energy storage, Chemelectrochem 2 (2015) 119—126.